ELSEVIER

J. Non-Newtonian Fluid Mech. 133 (2006) 14–27

Journal of Non-Newtonian Fluid Mechanics

www.elsevier.com/locate/jnnfm

Asymptotic basis of the L closure for finitely extensible dumbbells in suddenly started uniaxial extension

Ludwig C. Nitsche*, Weidong Zhang, Lewis E. Wedgewood

Department of Chemical Engineering, University of Illinois at Chicago, 810 South Clinton Street, Chicago, IL 60607, USA

Received 28 May 2005; received in revised form 29 September 2005; accepted 1 October 2005

Abstract

This paper applies the recent L closure [G. Lielens, P. Halin, I. Jaumain, R. Keunings, V. Legat, J. Non-Newtonian Fluid Mech., 76 (1998), 249–279], which was originally developed for FENE dumbbells with fixed friction, to two alternative dumbbell models of polymers in a dilute solution undergoing uniaxial extension: (A) a linear-locked dumbbell with fixed friction and (B) a FENE dumbbell with variable friction. The simplified box-spike representation of the probability density function (PDF) – used for Model B to close conformational averages of nonlinear quantities in terms of a reduced set of state variables (moments of the PDF) – is justified through detailed asymptotic analysis (singular perturbations combined with multiple scales) of the Smoluchowski equation, in the limit of large extensibility parameter at fixed elongation rate. Both dumbbell models A and B are actually more amenable to the L closure than the FENE to which it had previously been applied. The resulting closure relations compare favorably with corresponding integrals of asymptotic or numerical PDF's (the latter obtained via atomistic SPH simulations of the Smoluchowski equation). Example calculations show the L closure to yield reasonably accurate stress–extension curves, even for a moderate (dimensionless) limit of extension ($L = 4$).

Keywords: FENE dumbbell; Linear-locked dumbbell; L closure; Variable friction; Dilute polymer solution; Rheology; Singular perturbations; Multiple scales; Atomistic SPH

1. Introduction

For the rheology of dilute solutions of FENE dumbbells, recent work by Lielens and coworkers [8,16] has proposed a new "L closure" whereby the one-dimensional probability density function (PDF) is approximated with a simple class of shapes: a rectangular central section terminated with a delta function spike. The two-parameter family of shapes defined by this *ansatz* represents a canonical subspace of all possible PDF's, for which the second and fourth moments (state variables) can be related to the relevant geometric parameters (location and relative magnitude of the delta function). When the Smoluchowski equation is averaged against appropriate spatial weights to extract evolution equations for the state variables, the resulting nonlinear integrals are evaluated using the simplified PDF, thereby relating them to the state variables via the intermediaries of the geometric parameters. Thus, the evolution equations are closed consistently within the two-parameter state space, and can be solved much more easily than: (1) solving the Smoluchowski equation for the full PDF and then (2) integrating this PDF to obtain the moments at each time. The success of the scheme hinges on the fidelity with which the canonical family of shapes represents the actual progression of the PDF as governed by the Smoluchowski equation. Lielens et al. [8] formulated their canonical subspace using knowledge of the time evolution of the actual PDF, which was obtained from stochastic simulations (cf. [12,7]). The three-dimensional case has been addressed by decoupling the orientational and length dependences of the PDF in a multiplicative fashion, and the rectangular core has been further simplified (FENE-LS) by concentrating it into a second delta function [9].

Lielens et al. [8] were originally motivated by canonical distribution subspaces applied to the rheology of fiber suspensions [23]. Systematic selection of state variables based upon a maximum entropy principle [5] and applications to liquid crystalline polymers [6] have been developed more recently. Hysteresis loops in the stress–extension plane are observed in transient elongation, because different PDF's in the stretching

* Corresponding author. Tel.: +1 312 996 3469; fax: +1 312 996 0808.
E-mail address: lcn@uic.edu (L.C. Nitsche).

0377-0257/$ – see front matter © 2005 Elsevier B.V. All rights reserved.
doi:10.1016/j.jnnfm.2005.10.004

versus relaxing phases can be characterized by the same value of the second moment, while leading to different stresses [26,28,20,16]. At least a second-order closure is required to capture this feature. A one-parameter family of PDF's will necessarily lock the stress and extension together in a single-valued dependence.

To determine under which circumstances the L closure represents a rigorous approximation of the PDF, we apply singular perturbation theory to the Smoluchowski equation, in the asymptotic limit of a large extensibility parameter. For a sudden start of elongation, a narrow peak in probability density at or near the limit of extension is the inner solution (boundary layer), and the initially wide and ever broadening central core of probability is the outer solution. This disparity of lengthscales is accompanied by a separation of timescales between the slow rate of arrival of probability at the end and its rapid rearrangement within the boundary layer—as treated with the method of multiple scales. While the flow is on, the boundary layer does not move, which predetermines one parameter (location of the delta function) in the L closure, and thereby reduces it to first order. Interestingly, the FENE dumbbell with fixed friction (to which the L closure has hitherto been applied) does not exhibit an asymptotically narrow peak, so the delta function spike is not rigorously justified as an approximation. Lielens et al. [8] addressed this issue by augmenting the canonical subspace of PDF's with an additional parameter to describe a terminal spike that was widened into a rectangle. However, two other models do have the desirable asymptotic structure: (A) the linear-locked dumbbell with fixed friction and (B) the FENE dumbbell with variable friction. In the former case we obtain a uniformly valid asymptotic solution for the full PDF, which allows a very detailed consideration of the assumptions underlying the L closure.

1.1. Dumbbell models for dilute polymer solutions

The rheology of a dilute polymer solution is determined by the interaction of a single polymer chain with the surrounding liquid. A micro-mechanical model of a polymer molecule should capture two main features: (1) spatial extent of the frictional grip that the macromolecular chain exerts upon the fluid, whereby the chain straddles spatial variations in the flow field and thereby experiences deforming hydrodynamic forces; (2) resistance of the chain to deformation by the surrounding flow, which changes the macroscopic rheology from that of the Newtonian solvent when added up over all dissolved chains. The ubiquitous elastic dumbbell model [1,20,17,12,25,7,19,14,4,30] captures both features in a crude but effective manner that is readily amenable to analytical and numerical modeling. The beads represent two centers of hydrodynamic friction which can be pulled in different directions by the flow field. The resistance to unraveling and stretching of a real coiled macromolecule is primarily of entropic origin, for which the spring law represents an enthalpic substitute, and should be finitely extensible to prevent unbounded stretching of the dumbbell in strong flows [1,24,26,28]. The state of the dumbbell at any instant is described in statistical terms, by a probability density function defined on the space of internal (conformational) degrees of freedom: orientation and length. Macroscopic properties of the polymer solution – in particular viscosities in various types of viscometric flows and normal stress differences – are calculable from the PDF. Depending upon the particular dumbbell model and any assumptions or approximations employed to solve for the PDF—the resulting rheology includes non-Newtonian (shear thinning) behavior and transients such as hysteresis loops in the stress–extension plane [8,9,16,20,17].

Kinetic theory of dilute polymer solutions is mainly based upon an advection–diffusion or Smoluchowski equation (Fokker–Planck equation in the strongly damped limit [3]), which balances local accumulation of probability in each conformational state with fluxes due to the spring force, the hydrodynamic force exerted by the fluid on the beads and diffusion [1,12]. This paper treats a one-dimensional dumbbell model, wherein both beads are confined to the axis of a uniaxial elongational flow (cf. [7,8,20]). In the absence of vorticity, rotary modes play only a minor role, or else they can be decoupled at least approximately [9,17].

To motivate the mechanistic issues and closure approximations that figure in the relevant literature, it is useful first to describe the qualitative behavior of the PDF, which has been elucidated by Keunings [7], Lielens et al. [8,9] and Szeri [17] using stochastic simulations for a FENE dumbbell with the Warner form of the spring law. Here, we elaborate on their observations based upon the asymptotic analysis that is the subject of this paper. Starting at equilibrium, the PDF will be a mound-shaped (roughly Gaussian) peak, which represents a balance between Brownian fluctuations tending to extend the dumbbell and the restoring force of the spring. A sufficiently strong elongational flow (abruptly started) overpowers the central, linear regime of the spring, and pulls probability outward. The probability density away from the ends eventually decays to zero *as if* there were no stop in the spring, and whatever probability *would have* extended beyond the limit of extension at any time gets rearranged into a thin boundary layer at or near the limit of extension. There is a separation of timescales, whereby the boundary layer equilibrates to the incoming probability density much faster than the central peak drains off into the boundary layer.

At the final steady state, the actual finitely extensible PDF accumulates all of the probability at the end, whereas any Gaussian PDF must necessarily extend beyond the limit of extension [7,17]. Thus, it seems surprising that simple closure approximations (e.g., FENE-P) or averaging schemes based upon a Gaussian PDF actually do yield an accurate terminal stress [1]. But transient stresses hinge on the details of the evolution of the PDF, and are poorly predicted by Gaussian models or closures [7]. The comprehensive asymptotic analysis developed here, which combines singular perturbations and multiple scales: (1) formalizes and quantifies the qualitative description given above and (2) motivates the very simple but effective L closure representation of the PDF (rectangle terminated with a delta function near the limit of extension) that leads, at larger extensions, to linear closure relations between relevant averages of the PDF and the second moment (see Lielens et al. [8,9]).

1.2. Spring and drag laws

In this paper we consider two structural features of dumbbell models that have a major impact on the rheology of a dilute solution, as calculated for the one-dimensional case:

(1) *Finitely extensible spring law*: We will compare the Tanner model – a Hookean spring with rigid stops at the limit of extension [21,18,1] – with the FENE dumbbell [1,28,7].
(2) *Drag law*: We will compare a constant friction factor for the beads with an empirical, linear configuration-dependent friction law [19,15] that represents the increasing frictional grip that the surrounding liquid has on the polymer chain as the latter gets stretched [2,4,14].

Among the four possible combinations involving these two features, which are treated in the Ph.D. thesis of Zhang [29], only the FENE dumbbell with fixed friction does not share the separation of inner and outer timescales described above, and is not amenable to the same kind of asymptotic analysis. This paper is confined to the simplest and most complicated cases:

- *Model A*: Linear-locked spring; fixed drag.
- *Model B*: FENE spring; linear dependence of drag upon extension.

The configuration-dependent friction term can vary by an order of magnitude or more, depending upon the fully extended length of the chain. Any correction for hydrodynamic interactions would be comparatively minor, and is here neglected according to the freely draining dumbbell assumption.

1.3. Closure approximations and averaging schemes

To obtain a macroscopic characterization (mean-square extension, stress, etc.) the Smoluchowski equation is contracted into its second-moment form by a suitable integration over conformations, based upon the premise of a Gaussian PDF. This leads to an ODE for the second-moment tensor. In the presence of a nonlinear spring and/or variable drag, two main approaches have emerged to deal with the resulting nonlinear terms, whose averages cannot be closed in terms of the second moment: (i) closure approximations and (ii) averaging schemes.

1.3.1. Peterlin closure (PC)

For a FENE dumbbell with a constant drag coefficient, Peterlin [13] made a convenient, but not rigorously justifiable, mathematical ansatz in the second-moment equations: the ensemble average of a ratio was replaced by a ratio of ensemble averages. The effect of the ansatz was to close the second-moment equation and lead to a closed-form rheological constitutive equation for the "approximate" model. Convenience came at the price of inconsistency: interchanging the order of averaging and division is not rigorously correct even for a Gaussian PDF, and the discrepancy is typically not small in numerical practice or in any nontrivial asymptotic limit. While the exact FENE model constrains the end-to-end distance to be less than some maximum L, the effect of the Peterlin approximation is to soften the constraint to limit only the root-mean-square end-to-end distance to L, thereby allowing the tails of the PDF to extend to infinitely. An additional complication of the approximate model is that the second-moment equation is rendered nonlinear and now admits multiple steady states [2] in contrast to the exact model [28], which predicts a single steady state. A similar Peterlin-like approximation was applied to a dumbbell with variable drag [15]. Again, the effect was to close the second-moment equation; however, again the mathematical ansatz led to nonphysical multiple steady states [28].

Averaging schemes linearize the Smoluchowski equation by replacing the nonlinear, configuration-dependent diffusion tensor with an averaged version that is independent of configuration, and thus yield a Gaussian PDF as the solution. The ensemble-averaged diffusion tensor is calculated by integrating the configuration-dependent diffusion tensor against a PDF which is also assumed to be Gaussian, and the distinction between averaging methods lies in the source of this PDF and its relation to the Gaussian PDF actually being solved for.

1.3.2. Equilibrium averaging (EA)

For dumbbells with hydrodynamics interaction (a form of variable drag), Zimm [31] decoupled the PDF being solved for from the PDF used to obtain the averaged diffusion tensor. For the latter he employed the PDF for equilibrium in the absence of flow. This procedure leads to a linear second-moment equation and gives results that are reasonable in the limit of small-displacement flows. However, equilibrium averaging inconsistently removes all of the flow dependence in the variable drag.

1.3.3. Consistent averaging (CA)

As an improvement upon equilibrium averaging, the consistent averaging method [11,27] bases the averaged diffusion tensor upon a Gaussian PDF whose second moment coincides with the second moment being solved for when the Smoluchowski equation is contracted to an ODE. This enhanced level of internal consistency leads to qualitatively improved predictions of some material properties; however, the consistent-averaging method still fails quantitatively, even predicting the wrong sign of some properties.

1.3.4. Gaussian closure (GC)

The most successful, and chronologically latest, approach returned to the idea of closure, but with a sounder justification than an ad hoc ansatz [25,32]. To estimate the ensemble averages appearing in the second-moment form of the Smoluchowski equation for a Hookean dumbbell, a Gaussian PDF was used—based in a consistent manner on the same second-moment tensor being solved for. The conformational integrals had to be carried out numerically. Although the solution to the full, nonlinear Smoluchowski equation is not actually Gaussian, this simple ansatz leads to excellent predictions for material functions.

1.3.5. The L closure (LC)

For expressing the nonlinear averages in terms of the state variables, the L closure [8,9,16] proceeds consistently by the

same basic premise as the Gaussian closure, but replaces the Gaussian PDF with the characteristic box-spike shape that more accurately represents the actual PDF, while also being more tractable analytically. Rheological predictions of the scheme near the initial equilibrium and the terminal steady state have been improved by augmenting and modifying the canonical subspace as follows: (i) replacing the flat central core with a Gaussian distribution and (ii) widening the delta function spike into a rectangle [8]. But such complications seem to propel the approach of closure to the point of diminishing returns. In this paper we justify the assumptions of the L closure with reference to the asymptotic structure of the Smoluchowski equation.

2. Governing kinetic equation

Posed in dimensionless form, and reduced to half of the original domain by symmetry, the Smoluchowski equation governing the probability density in one-dimensional conformation space (extension x of the spring) of a finitely extensible dumbbell confined to the axis of a uniaxial elongational flow is [7,19,1]

$$\frac{\partial P}{\partial t} + \frac{\partial J}{\partial x} = 0, \qquad J = VP - D\frac{\partial P}{\partial x} \quad (0 < x < L) \tag{1}$$

The advective and diffusive coefficients for the two models are as follows [20,19,1,15]:

$$\text{Model A:} \quad V(x) = \left(\gamma - \frac{1}{2}\right)x, \qquad D(x) = \frac{1}{2} \tag{2}$$

$$\text{Model B:} \quad V(x) = \left(\gamma - \frac{1}{2}\frac{1}{1+kx}\frac{1}{1-x^2/L^2}\right)x,$$
$$D(x) = \frac{1}{2}\frac{1}{1+kx} \tag{3}$$

Here, γ is an appropriately reduced elongation rate, which must exceed 1/2 in order for the flow to stretch the spring appreciably toward its limit of extension. Illustrative numerical calculations in this paper will be restricted to $\gamma = 1$. The factor $1 + kx$ appearing in the denominators for Model B represents an empirical estimate for the increase in the friction coefficient of the dumbbell as it becomes extended. The constant k ranges from 0.02 to $\sqrt{2}/2$ [15]. No-flux conditions at both ends of the domain take care of symmetry and finite extensibility, respectively.

$$J = 0 \quad \text{at } x = 0, L \tag{4}$$

Although the FENE factor $(1 - x^2/L^2)^{-1}$ does, in principle, render the no-flux condition superfluous at the right end, this condition is retained in the numerical solutions.

The Smoluchowski equation (1) admits simplification in the asymptotic limit of a long dumbbell ($L \to \infty$), for which we define the small perturbation parameter $\epsilon = L^{-1} \ll 1$.

3. Asymptotics for the linear-locked dumbbell with fixed friction

For the linear Smoluchowski equation

$$\frac{\partial P}{\partial t} + \frac{\partial}{\partial x}\left\{\left(\gamma - \frac{1}{2}\right)xP - \frac{1}{2}\frac{\partial P}{\partial x}\right\} = 0, \quad 0 < x < \epsilon^{-1} \tag{5}$$

the initial condition is equilibrium with no flow ($\gamma = 0$). For a sufficiently long spring ($\epsilon \ll 1$) the Gaussian profile

$$P(x, 0) \sim \sqrt{\frac{2}{\pi}}\, \mathrm{e}^{-x^2/2} \tag{6}$$

has only exponentially small errors in the normalization factor and no-flux condition (4). The final steady-state PDF is

$$P(x, \infty) = \left\{\int_0^{\epsilon^{-1}} \mathrm{e}^{(\gamma-1/2)x^2}\, \mathrm{d}x\right\}^{-1} \mathrm{e}^{(\gamma-1/2)x^2}$$
$$= \left(\frac{2\gamma - 1}{\epsilon}\right)\left(1 - \frac{\epsilon^2}{2\gamma - 1} + \mathrm{O}(\epsilon^4)\right) \mathrm{e}^{(\gamma-1/2)(x^2-\epsilon^{-2})} \tag{7}$$

3.1. Exact outer solution (Hookean dumbbell)

After the elongational flow is turned on, one can obtain an exact solution to Eq. (5) by assuming that the PDF maintains its Gaussian form. This will satisfy the symmetry condition (4) at $x = 0$ but not the no-flux condition at the end—which is the job of the inner solution to which the Gaussian form is matched.

Enforcing normalization of total probability at all times, which includes the portion of the PDF extending (unphysically) beyond the stop of the spring, we use the trial solution

$$P^{[\mathrm{O}]}(x, t) = \frac{1}{\ell(t)}\sqrt{\frac{2}{\pi}}\, \exp\left\{-\frac{1}{2}\left[\frac{x}{\ell(t)}\right]^2\right\} \tag{8}$$

wherein $\ell(t)$ is directly related to the second moment:

$$\langle x^2 \rangle = \ell(t)^2 \tag{9}$$

Substituting Eq. (8) into the PDE (5), we find the ODE and initial condition for $\ell(t)$.

$$\frac{\mathrm{d}\ell}{\mathrm{d}t} = \left(\gamma - \frac{1}{2}\right)\ell(t) + \frac{1}{2\ell(t)}, \quad \ell(0) = 1 \tag{10}$$

The solution is

$$\ell(t) = \left\{\left(1 + \frac{1}{2\gamma - 1}\right)\mathrm{e}^{(2\gamma-1)t} - \frac{1}{2\gamma - 1}\right\}^{1/2} \tag{11}$$

Advection and diffusion are of comparable importance when $\ell = \mathrm{ord}(1)$, but advection dominates when $\ell = \mathrm{ord}(\epsilon^{-1})$.

3.2. Contraction to the second moment

Consistent averaging and the Gaussian closure are equivalent for Model A, and recover the exact solution (8). The general procedure is briefly reviewed here by way of preparing for subsequent complications associated with the FENE and variable drag terms of dumbbell Model B.

We start by integrating the PDE (5) against x^2 over the infinite interval $0 < x < \infty$, which ignores finite extensibility.

$$\int_0^\infty x^2 \frac{\partial P}{\partial t}\,\mathrm{d}x = -\int_0^\infty x^2\,\mathrm{d}J \tag{12}$$

The time derivative is pulled outside the first integral, and the flux integral is done by parts to yield an equation directly for the second moment of the PDF:

$$\frac{\mathrm{d}\langle x^2\rangle}{\mathrm{d}t} = -x^2 J|_0^\infty + \int_0^\infty 2xJ\,\mathrm{d}x \tag{13}$$

The symmetry and no-flux conditions (4) dispose of the upper and lower limits. We now explicitly write the advective and diffusive contributions to the flux J, and integrate by parts again for the diffusive term, to obtain

$$\frac{\mathrm{d}\langle x^2\rangle}{\mathrm{d}t} = 2\langle xV(x)\rangle + 2\left\langle \frac{\mathrm{d}}{\mathrm{d}x}[xD(x)]\right\rangle \tag{14}$$

This is the general starting point for arbitrary forms of the advective and diffusive terms.

With a linear velocity and constant diffusivity, the conformational averages can be closed exactly to obtain

$$\frac{\mathrm{d}\langle x^2\rangle}{\mathrm{d}t} = (2\gamma-1)\langle x^2\rangle + 1, \quad \langle x^2\rangle = 1 \text{ at } t = 0 \tag{15}$$

There are two routes for calculating $\ell(t)$. First, one can solve the ODE (15) for $\langle x^2\rangle(t)$, and then take $\ell(t) = \sqrt{\langle x^2\rangle(t)}$ on a post facto basis. Alternatively, the ODE (15) can be transformed into an ODE directly for $\ell(t)$,

$$\frac{\mathrm{d}\ell}{\mathrm{d}t} = \left[\frac{\mathrm{d}\langle x^2\rangle}{\mathrm{d}\ell}\right]^{-1}[(2\gamma-1)\langle x^2\rangle + 1] = \frac{1}{2\ell}[(2\gamma-1)\ell^2 + 1] \tag{16}$$

thereby recovering Eq. (10). Both approaches give the same result for $\ell(t)$.

3.3. General features of the outer solution

The Gaussian outer solution does not satisfy the constraint on maximum extension. This peak is ord(1) in height while it extends over an ord(1) width in x, which characterizes the initial equilibrium distribution. By the time it has spread near the stop of the spring ($x = \epsilon^{-1}$), its height has decayed to O(ϵ), which is as far as we shall go in matching to the inner solution.

As will be seen below, the most important feature of the outer solution is the amount $A(t)$ of probability that extends beyond the stop of the spring:

$$A(t) = \int_{\epsilon^{-1}}^\infty P^{[\mathrm{O}]}(x,t)\,\mathrm{d}x = 1 - \int_0^{\epsilon^{-1}} P^{[\mathrm{O}]}(x,t)\,\mathrm{d}x \tag{17}$$

If the outer solution adopts the Gaussian form (8) then

$$A(t) = \operatorname{erfc}\left\{\frac{1}{\ell(t)\epsilon\sqrt{2}}\right\} \tag{18}$$

For future reference we note the derivative formula

$$A'(t) = \frac{1}{[\ell(t)]^2\epsilon\sqrt{2\pi}}\left[(2\gamma-1)\ell(t) + \frac{1}{\ell(t)}\right]\exp\left\{\frac{-1}{2\epsilon^2[\ell(t)]^2}\right\} \tag{19}$$

For matching with the subsequent inner solution, we can derive one particular relation between $A(t)$ and the end value of the outer solution directly from the Smoluchowski equation (5). Noting that

$$A'(t) = -\int_0^{\epsilon^{-1}} \frac{\partial P}{\partial t}\,\mathrm{d}x = \left[\left(\gamma - \frac{1}{2}\right)xP - \frac{1}{2}\frac{\partial P}{\partial x}\right]_0^{\epsilon^{-1}} \tag{20}$$

we find

$$P^{[\mathrm{O}]}_{\mathrm{end}}(t) = \frac{\epsilon}{\gamma - \frac{1}{2}}\left\{A'(t) + \frac{1}{2}\left.\frac{\partial P}{\partial x}\right|_{\mathrm{end}}\right\} \tag{21}$$

By the time the end probability builds up to appreciable magnitude, $\partial P/\partial x$ is O(ϵ^2), and so negligible. Before then, the end probability is negligible. Thus, we have

$$P^{[\mathrm{O}]}_{\mathrm{end}}(t) \approx \epsilon\left\{\frac{A'(t)}{\gamma - \frac{1}{2}}\right\} \tag{22}$$

3.4. Stretched boundary-layer coordinate

Only the stop in the spring prevents the outflux of probability from the end, $x = \epsilon^{-1}$. The steady-state solution (7) suggests a peak of width of ord(ϵ). Thus, we define the inner coordinate η,

$$x = \epsilon^{-1} + \epsilon\eta, \quad -\infty < \eta \le 0 \tag{23}$$

Rewriting the PDE (10) in terms of η we find

$$\epsilon^2\frac{\partial P^{[\mathrm{I}]}}{\partial t} + \frac{\partial}{\partial \eta}\left\{\left[\left(\gamma - \frac{1}{2}\right)P^{[\mathrm{I}]} - \frac{1}{2}\frac{\partial P^{[\mathrm{I}]}}{\partial \eta}\right] + \epsilon^2\eta P^{[\mathrm{I}]}\right\} = 0 \tag{24}$$

On the inner lengthscale the advective flux toward the (impenetrable) end is balanced by a diffusive counterflux of the same order.

3.5. Two-timescale expansion for the inner solution

The scaling of the time derivative suggests a rapid equilibration to a pseudo-steady, piled-up boundary layer, with the total accumulated probability being determined by what arrives more slowly from the outer solution. This idea can be formalized using a two-timescale expansion for the inner solution:

$$P^{[\mathrm{I}]}(\eta,t;\epsilon) \sim \epsilon^{-1}P_0^{[\mathrm{I}]}(\eta,\tau,T) + \epsilon P_1^{[\mathrm{I}]}(\eta,\tau,T) + \epsilon^3 P_2^{[\mathrm{I}]}(\eta,\tau,T) + \cdots \tag{25}$$

with the respective fast and slow time variables

$$\tau = \epsilon^{-2}t, \qquad T = t \tag{26}$$

The two-timescale expansion begins at order ϵ^{-1}, in order that the inner solution can accumulate ord(1) probability within a

peak of ord(ϵ) width, and ascends in powers of ϵ^2, since this is the only form in which ϵ appears in the inner PDE.

Substituting the expansion (20) into the inner PDE written in both time variables

$$\left\{\frac{\partial P^{[\mathrm{I}]}}{\partial \tau}+\frac{\partial}{\partial \eta}\left[\left(\gamma-\frac{1}{2}\right)P^{[\mathrm{I}]}-\frac{1}{2}\frac{\partial P^{[\mathrm{I}]}}{\partial \eta}\right]\right\} + \epsilon^2\left\{\frac{\partial P^{[\mathrm{I}]}}{\partial T}+\eta P^{[\mathrm{I}]}\right\}=0 \tag{27}$$

and collecting terms of like powers of ϵ, we obtain a hierarchy of PDE's in η and τ, with the slow time variable T appearing as a parameter.

$$\frac{\partial P_0^{[\mathrm{I}]}}{\partial \tau}+\left(\gamma-\frac{1}{2}\right)\frac{\partial P_0^{[\mathrm{I}]}}{\partial \eta}-\frac{1}{2}\frac{\partial^2 P_0^{[\mathrm{I}]}}{\partial \eta^2}=0 \tag{28}$$

$$\frac{\partial P_1^{[\mathrm{I}]}}{\partial \tau}+\left(\gamma-\frac{1}{2}\right)\frac{\partial P_1^{[\mathrm{I}]}}{\partial \eta}-\frac{1}{2}\frac{\partial^2 P_1^{[\mathrm{I}]}}{\partial \eta^2} =-\frac{\partial P_0^{[\mathrm{I}]}}{\partial T}-\left(\gamma-\frac{1}{2}\right)\frac{\partial}{\partial \eta}\left[\eta P_0^{[\mathrm{I}]}\right] \tag{29}$$

The boundary condition for $P_0^{(\mathrm{I})}$ as $\eta\to-\infty$ is obtained by integrating Eq. (28) over η. In order to avoid accumulation of probability on the short timescale we must set

$$0=\frac{\partial}{\partial \tau}\int_0^\infty P_0^{(\mathrm{I})}(\eta,\tau,T)\,\mathrm{d}\eta=\left[\left(\gamma-\frac{1}{2}\right)P_0^{(\mathrm{I})}-\frac{1}{2}\frac{\partial P_0^{(\mathrm{I})}}{\partial \eta}\right]_{-\infty}^{0} \tag{30}$$

The upper limit vanishes because of the no-flux condition at the stop of the spring, so it follows that the flux must also vanish in the limit as $\eta\to-\infty$. Thus, we obtain

$$P_0^{[\mathrm{I}]}(\eta,\tau,T)=P_0^{[\mathrm{I}],\infty}(\eta,T)+\{\tau\text{-timescale decay terms}\} \tag{31}$$

with

$$P_0^{[\mathrm{I}],\infty}(\eta,T)=A(T)\lambda\,\mathrm{e}^{\lambda\eta}\quad(\lambda=2\gamma-1) \tag{32}$$

The prefactor $A(T)$ represents precisely the total probability contained within the leading-order peak, and so it could be obtained simply from an overall normalization: whatever area extends beyond the end from the Gaussian outer solution goes into $A(T)$ as given by Eq. (18). More rigorously, one can integrate the first-order Eq. (29) in η to conclude that

$$\begin{aligned}\frac{\partial}{\partial \tau}\int_{-\infty}^{0}P_1^{[\mathrm{I}]}(\eta,\tau,T)\,\mathrm{d}\eta &=-\frac{\partial}{\partial T}\int_{-\infty}^{0}P_0^{[\mathrm{I}]}(\eta,\tau,T)\,\mathrm{d}\eta\\ &\quad-\left[\left(\gamma-\frac{1}{2}\right)P_1^{[\mathrm{I}]}-\frac{1}{2}\frac{\partial P_1^{[\mathrm{I}]}}{\partial \eta}+\left(\gamma-\frac{1}{2}\right)\eta P_0^{[\mathrm{I}]}\right]_{-\infty}^{0}\end{aligned} \tag{33}$$

To avoid secular accumulation of probability at first order we must require that

$$A'(T)=\left[\left(\gamma-\frac{1}{2}\right)P_1-\frac{1}{2}\frac{\partial P_1}{\partial \eta}\right]_{-\infty} \tag{34}$$

In other words, the slow-timescale rate at which probability accumulates within the leading-order inner solution equals the incoming flux at first order. The latter is of ord(1), which matches the advective flux from the leading *outer* solution near the boundary layer (see Eq. (22)). Thus, we should cut off from the outer solution – a Gaussian peak that expands on the slow-timescale – whatever extends beyond the limit of extension, and rearrange that amount of probability into a "piled-up" boundary layer using the pseudo-steady exponential solution (32). This justifies identifying the inner, slow-timescale function $A(T)$ with the outer quantity defined by Eq. (18).

Instead of integrating the second-order equation in order to determine the T-dependent coefficients appearing in $P_1^{[\mathrm{I}]}$, we shall be content with the simpler normalization argument, which should give an equivalent result. The quasi-steady solution at first order is

$$P_1^{[\mathrm{I}],\infty}(\eta,T)=\left[\left(\frac{\lambda^2}{2}A(T)\right)\eta^2+(2A'(T))\eta+\left(\frac{2}{\lambda}A'(T)-A(T)\right)\right]\mathrm{e}^{\lambda\eta}+B(T) \tag{35}$$

Note that the bracketed term gives zero net probability when integrated in η. Matching Eq. (35) to the outer solution determines the free coefficient $B(T)$. From Eq. (22) we see that

$$\lim_{\eta\to-\infty}\epsilon P_1^{[\mathrm{I}],\infty}(\eta,T)=\epsilon B(T)=\epsilon\left\{\frac{2A'(T)}{\lambda}\right\} \tag{36}$$

3.6. Uniformly valid asymptotic solution

Constructing the uniformly valid solution is relatively simple in this case, because the common limiting behavior (inner limit of outer solution and outer limit of inner solution) is just a constant, given by Eq. (22). Combining Eqs. (8), (32) and (35), we find

$$\begin{aligned}P(x,t)\sim{}&\frac{1}{\ell(t)}\sqrt{\frac{2}{\pi}}\exp\left\{-\frac{1}{2}\left[\frac{x}{\ell(t)}\right]^2\right\}+\epsilon^{-1}\operatorname{erfc}\left\{\frac{1}{\ell(t)\epsilon\sqrt{2}}\right\}\\ &\times(2\gamma-1)\exp\left\{(2\gamma-1)\left(\frac{x-\epsilon^{-1}}{\epsilon}\right)\right\}\\ &+\epsilon\left\{\left[\frac{(2\gamma-1)^2}{2}A(t)\right]\left(\frac{x-\epsilon^{-1}}{\epsilon}\right)^2+[2A'(t)]\left(\frac{x-\epsilon^{-1}}{\epsilon}\right)\right.\\ &\left.+\left[\frac{2}{2\gamma-1}A'(t)-A(t)\right]\right\}\\ &\times\exp\left\{(2\gamma-1)\left(\frac{x-\epsilon^{-1}}{\epsilon}\right)\right\}+\mathrm{O}(\epsilon^2)\end{aligned} \tag{37}$$

with $A(t)$ and $\acute{A}(t)$ given by Eqs. (18) and (19).

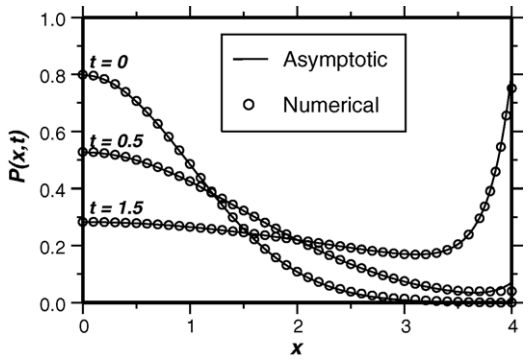

Fig. 1. PDF's for a linear-locked dumbbell with fixed drag (Eq. (5)). Comparison of the asymptotic solution (37) with numerical PDFs calculated using ASPH. Here, $\gamma = 1$ and $\epsilon = 0.25$.

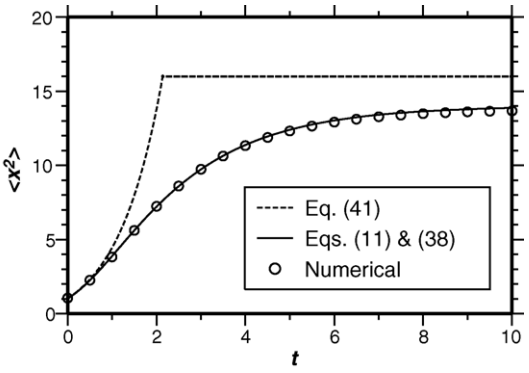

Fig. 2. Time evolution of the second moment for a linear-locked dumbbell with fixed drag. The asymptotic formula (38) is compared with the numerical solution. Results are also shown for the consistently averaged second-moment Eq. (41).

For elongation rate $\gamma = 1$ and a fairly short spring ($L = 4$, $\epsilon = 0.25$), Fig. 1 presents a comparison of the asymptotic solution (37) with numerical PDF's obtained by applying a particle method called atomistic smoothed particle hydrodynamics (ASPH) to the Smoluchowski equation (5) (see Nitsche and Zhang [10] for a general description of the method for two-dimensional advection–diffusion problems). In brief, ASPH tracks a swarm of particles that move deterministically according to the local advective flux and also a relative diffusional velocity due to a suitably formulated mutual repulsion among a localized subset of particles. A weight-function average extracts the local density of particles to yield the PDF. The calculations reported here are essentially the same as those presented in the Ph.D. thesis of Zhang [29]. We used 250 particles in all, with roughly 20 particles in each local sum. (For the FENE with variable friction (Fig. 5), the corresponding parameters were 500 and 30.) Even though the spring is not very long, the asymptotic PDF's are very accurate, and illustrate how probability drains from the central Gaussian peak into a boundary layer of approximately exponential shape at the limit of extension.

3.7. Second moment

In order to approximate integral properties of the PDF consistently at leading order, we need only the first two lines in the asymptotic solution (37), because the ord(ϵ) inner correction contributes negligibly when integrated over the ord(ϵ) boundary layer. Here, we consider the second moment of the PDF, which indicates the degree of stretching. In two or three dimensions, the second moment would yield information on birefringence [16,8].

$$\langle x^2\rangle \sim \underbrace{\left\{\ell^2 \operatorname{erf}\left(\tfrac{1}{\epsilon\ell\sqrt{2}}\right) - \tfrac{\ell}{\epsilon}\sqrt{\tfrac{2}{\pi}}\,\exp\left(\tfrac{-1}{2\epsilon^2\ell^2}\right)\right\}}_{\text{central Gaussian}} + \underbrace{\left\{\left(\tfrac{1}{\epsilon^2} - \tfrac{2}{2\gamma-1}\right)\operatorname{erfc}\left(\tfrac{1}{\epsilon\ell\sqrt{2}}\right)\right\}}_{\text{boundary layer}} \tag{38}$$

The leading boundary-layer contribution in Eq. (38) comes from regarding all of the associated probability concentrated at the limit of extension of the spring—as though the exponential profile of ord(ϵ) width were replaced by a delta function centered at $x = \epsilon^{-1}$.

$$P(x,t) \approx \frac{1}{\ell(t)}\sqrt{\frac{2}{\pi}}\,\exp\left\{-\frac{1}{2}\left[\frac{x}{\ell(t)}\right]^2\right\} + \operatorname{erfc}\left\{\frac{1}{\ell(t)\epsilon\sqrt{2}}\right\}\delta(x-\epsilon^{-1}) \tag{39}$$

With ϵ held fixed, the asymptotic behavior as $\ell \to \infty$ is

$$\langle x^2\rangle \sim \epsilon^{-2}\left\{1 - \left(\frac{2}{3}\sqrt{\frac{2}{\pi}}\right)\frac{1}{\epsilon\ell}\right\} \tag{40}$$

Fig. 2 shows the second moment as a function of time, calculated by substituting Eq. (11) for $\ell(t)$ in the asymptotic formula (38). This asymptotic curve is in excellent agreement with results calculated from the full numerical solution of the PDE (5) (see Zhang [29]).

The consistently averaged second-moment Eq. (15) suffers from a defect when it is applied to the Tanner model: there is no way to incorporate the limit of extension, aside from artificially stopping the second moment when it runs into the hard stop of the spring:

$$\langle x^2\rangle = \begin{cases} \left(1 + \frac{1}{2\gamma-1}\right)\mathrm{e}^{(2\gamma-1)t} - \frac{1}{2\gamma-1}, & t < T \\ \epsilon^{-2}, & t \geq T \end{cases}$$

$$T = \frac{1}{2\gamma-1}\ln\left[\frac{2\gamma-1+\epsilon^2}{2\gamma\epsilon^2}\right] \tag{41}$$

The consistently averaged second moment rises too quickly, and levels off abruptly with a corner—because it does not incorporate the continuous drainage of the central Gaussian into the boundary layer. The terminal value does not account for finite thickness of the boundary layer, and represents only the leading ϵ^{-2} term in Eq. (38). This explains why consistent averaging overpredicts the long-time asymptote by $2/(2\gamma-1) = 2$, which can be read off from Fig. 2. The discrepancy is noticeable in this example because the limit of extension is not very large ($L = \epsilon^{-1} = 4$); it would become unimportant for significantly longer dumbbells. Thus, at steady state the deficiency of con-

sistent averaging (which is equivalent to the Gaussian closure in this simple case) remains largely hidden: only the transient reveals it.

3.8. The L closure: box-spike approximation of the PDF

The width parameter $\ell(t)$ that specifies the Gaussian peak in Eq. (39) at each instant can be replaced by an equivalent parameter: the (suitably scaled) probability density at $x = 0$:

$$Q(t) \stackrel{\text{def}}{=} \frac{P(0,t)}{\epsilon} = \frac{1}{\epsilon \ell(t)} \sqrt{\frac{2}{\pi}} \tag{42}$$

Eq. (38) can then be converted into a relation between $\langle x^2 \rangle$ and Q.

$$\epsilon^2 \langle x^2 \rangle \sim \left(\frac{2}{\pi Q^2}\right) \operatorname{erf}\left(\frac{Q\sqrt{\pi}}{2}\right) - \left(\frac{2}{\pi Q}\right) \exp\left(\frac{-\pi Q^2}{4}\right) + \operatorname{erfc}\left(\frac{Q\sqrt{\pi}}{2}\right) \tag{43}$$

The L closure of Lielens and coworkers [8,9,16] involves a very simple but useful model for the time-evolving PDF, which is suggested by the progression of curves in Fig. 1. By the time $P(0,t)$ has decayed to ord(ϵ), which means $Q(t) = \text{ord}(1)$, the Gaussian core is nearly constant over the domain $0 < x < \epsilon^{-1}$. Thus, we represent the PDF with a completely flat outer profile, which is augmented with the inner delta function from Eq. (39)—the latter being suitably weighted to preserve the total probability. At earlier times, when the outer solution has not yet reached the end, one can model the PDF with a rectangle.

$$P_{\mathrm{L}}(x,t) = \begin{cases} \epsilon Q[H(x) - H(x - [\epsilon Q]^{-1})], & Q \geq 1 \\ \epsilon Q[H(x) - H(x - \epsilon^{-1})] + (1 - Q)\delta(x - \epsilon^{-1}), & 0 \leq Q < 1 \end{cases} \tag{44}$$

with $H(x)$ the Heavyside unit step function. This L closure representation of the PDF is shown in Fig. 3, and the associated dependence of the second moment upon Q is as follows:

$$\epsilon^2 \langle x^2 \rangle_{\mathrm{L}} = \begin{cases} \frac{1}{3Q^2}, & Q \geq 1 \\ 1 - \frac{2Q}{3}, & Q < 1 \end{cases} \tag{45}$$

The linear dependence of $\epsilon^2 \langle x^2 \rangle$ upon Q when $Q < 1$ matches the first two terms in the Taylor expansion of Eq. (43) about $Q = 0$.

Based upon Eqs. (44) and (45), there is a piecewise linear relationship between the second moment and the total probability A accumulated in the delta function (see Fig. 4).

$$A = \begin{cases} 0, & 0 \leq \epsilon^2 \langle x^2 \rangle \leq \frac{1}{3} \\ -\frac{1}{2} + \frac{3}{2}\epsilon^2 \langle x^2 \rangle, & \frac{1}{3} \leq \epsilon^2 \langle x^2 \rangle \leq 1 \end{cases} \tag{46}$$

Letting Q run from 0 to $\epsilon^{-1}(2/\pi)^{1/2}$ in Eq. (43) and the suitable version of Eq. (18),

$$A = \operatorname{erfc}\left\{\frac{Q\sqrt{\pi}}{2}\right\} \tag{47}$$

we can obtain a corresponding asymptotic curve, which is seen in Fig. 4 to validate the simple approximation (46) quite well.

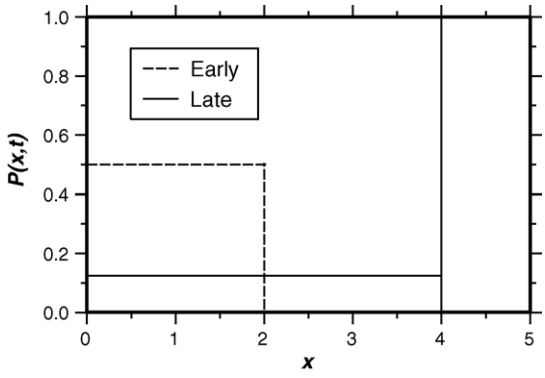

Fig. 3. A simplified box-spike representation of the PDF (Eq. (44)), according to the L closure of Lielens et al. [8]. The central peak is modeled as a rectangular pulse, and the boundary layer is modeled as a delta function located at the limit of extension. Probability starts accumulating in the delta function when the width of the rectangle reaches the length of the spring.

4. Asymptotics for the FENE dumbbell with variable friction

New elements in the Smoluchowski equation are: (i) the FENE factor in the spring law, which causes the restoring force to blow up as the spring stretches toward its limit of extension, and (ii) the empirical, configuration-dependent friction factor, which modifies the diffusive flux and that part of the advective flux that comes from the spring pulling back against the stretching flow.

$$\frac{\partial P}{\partial t} + \frac{\partial}{\partial x}\left\{\left(\gamma - \frac{1}{2}\frac{1}{1+kx}\frac{1}{1-\epsilon^2 x^2}\right) xP - \frac{1}{2}\frac{1}{1+kx}\frac{\partial P}{\partial x}\right\} = 0, \quad 0 < x < \epsilon^{-1} \tag{48}$$

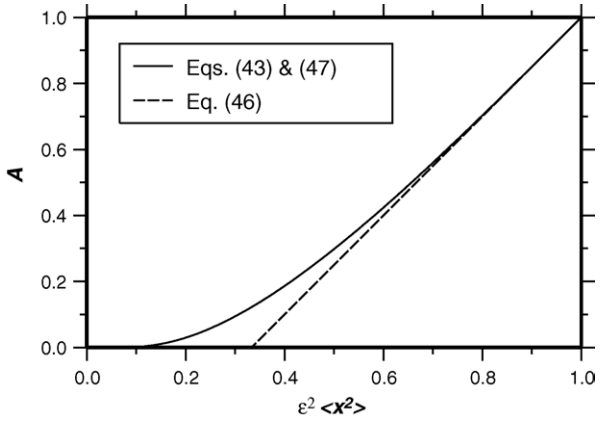

Fig. 4. Amount of probability A accumulated in the boundary layer vs. the scaled second moment for the linear-locked dumbbell with fixed drag. Rigorous asymptotics (Eqs. (43) and (47)), are compared with the simple approximate formula (46) resulting from the family of simplified box-spike PDF's (Fig. 3) from the L closure [8].

The FENE factor brings the limit of extension explicitly into the PDE, and nonlinear terms will require closure assumptions of some sort.

The initial equilibrium PDF is

$$P(x,0) = \left\{ \int_0^{\epsilon^{-1}} (1-\epsilon^2 x^2)^{1/2\epsilon^2}\, \mathrm{d}x \right\}^{-1} (1-\epsilon^2 x^2)^{1/2\epsilon^2} \quad (49)$$

and the final steady-state PDF is

$$P(x,\infty) = \left\{ \int_0^{\epsilon^{-1}} (1-\epsilon^2 x^2)^{1/2\epsilon^2}\, \mathrm{e}^{\gamma x^2(3+2kx)/3}\, \mathrm{d}x \right\}^{-1} \times (1-\epsilon^2 x^2)^{1/2\epsilon^2}\, \mathrm{e}^{\gamma x^2(3+2kx)/3} \quad (50)$$

Here, we will proceed less systematically than with dumbbell Model A, and develop first only as much of the boundary-layer structure as is required to motivate the L closure.

4.1. Stretched boundary-layer coordinate

The FENE factor in Eq. (48) causes probability to accumulate near that point $x = \lambda$ where the advective velocity vanishes:

$$\frac{V(\lambda;\epsilon)}{\lambda} = \gamma - \frac{1}{2}\left(\frac{1}{1+k\lambda}\right)\left(\frac{1}{1-\epsilon^2\lambda^2}\right) = 0 \quad (51)$$

An algebraic perturbation yields

$$\lambda(\epsilon) \sim \frac{1}{\epsilon} - \left(\frac{1}{4k\gamma}\right) + \left(\frac{8\gamma-3}{32k^2\gamma^2}\right)\epsilon - \left(\frac{(1-2\gamma)^2}{16k^3\gamma^3}\right)\epsilon^2 + \mathrm{O}(\epsilon^3) \quad (52)$$

The width of the final steady-state peak (50) scales with ϵ, which suggests the inner-variable scaling

$$x = \lambda + \eta\epsilon \quad (53)$$

Written in terms of η, the Smoluchowski equation (48) becomes

$$\epsilon\frac{\partial P}{\partial t} + \frac{\partial}{\partial\eta}\left[V(\eta;\epsilon)P - D(\eta;\epsilon)\frac{\partial P}{\partial\eta}\right] = 0 \quad (54)$$

with the advective and diffusive coefficients

$$V(\eta;\epsilon) = \left\{\gamma - \frac{1}{2}\left[\frac{1}{1+k(\lambda+\eta\epsilon)}\right]\left[\frac{1}{1-\epsilon^2(\lambda+\eta\epsilon)^2}\right]\right\} \times (\lambda+\eta\epsilon) \quad (55)$$

$$D(\eta;\epsilon) = \frac{1}{2\epsilon}\left[\frac{1}{1+k(\lambda+\eta\epsilon)}\right] \quad (56)$$

Local expansions of these functions about $\eta = 0$ take the form

$$V(\eta;\epsilon) = V_0(\eta) + \epsilon V_1(\eta) + \mathrm{O}(\epsilon^2) \quad (57)$$

$$D(\eta;\epsilon) = D_0(\eta) + \epsilon D_1(\eta) + \mathrm{O}(\epsilon^2) \quad (58)$$

with

$$V_0(\eta) = [-4k\gamma^2]\eta \quad (59)$$

$$V_1(\eta) = \left[4\gamma(1-\gamma)\right]\eta - [16k^2\gamma^3]\eta^2 \quad (60)$$

$$D_0(\eta) = \left[\frac{1}{2k}\right] \quad (61)$$

$$D_1(\eta) = \left[\frac{1-4\gamma}{8k^2\gamma}\right] \quad (62)$$

At leading order we have a linear velocity (equivalently, a harmonic binding potential) and a constant diffusivity. On this basis one would expect the inner solution to be a Gaussian peak.

4.2. Two-timescale expansion for the inner solution

As suggested by the ϵ factor multiplying the time derivative in Eq. (48), we use the two-timescale expansion

$$P^{[\mathrm{I}]}(\eta,t;\epsilon) \sim \epsilon^{-1}P_0^{[\mathrm{I}]}(\eta,\tau,T) + P_1^{[\mathrm{I}]}(\eta,\tau,T) + \epsilon P_2^{[\mathrm{I}]}(\eta,\tau,T) + \cdots \quad (63)$$

with the fast and slow time variables

$$\tau = \epsilon^{-1}t, \qquad T = t \quad (64)$$

Note that the disparity between timescales is one order lower than for dumbbell Model A (cf. Eq. (26)).

Substituting the expansion (63) into the inner PDE written in both time variables,

$$\left\{\frac{\partial P^{[\mathrm{I}]}}{\partial\tau} + \frac{\partial}{\partial\eta}\left[V_0(\eta)P^{[\mathrm{I}]} - D_0\frac{\partial P^{[\mathrm{I}]}}{\partial\eta}\right]\right\} + \epsilon\left\{\frac{\partial P^{[\mathrm{I}]}}{\partial T} + \frac{\partial}{\partial\eta}\left[V_1(\eta)P^{[\mathrm{I}]} - D_1\frac{\partial P^{[\mathrm{I}]}}{\partial\eta}\right]\right\} + \cdots = 0 \quad (65)$$

and collecting terms of like powers of ϵ, we obtain again a hierarchy of PDE's in η and τ, with the slow time variable T appearing as a parameter.

$$\frac{\partial P_0^{[\mathrm{I}]}}{\partial\tau} + \frac{\partial}{\partial\eta}\left[V_0(\eta)P_0^{[\mathrm{I}]} - D_0(\eta)\frac{\partial P_0^{[\mathrm{I}]}}{\partial\eta}\right] = 0 \quad (66)$$

$$\frac{\partial P_1^{[\mathrm{I}]}}{\partial\tau} + \frac{\partial}{\partial\eta}\left[V_0(\eta)P_1^{[\mathrm{I}]} - D_0(\eta)\frac{\partial P_1^{[\mathrm{I}]}}{\partial\eta}\right] = -\frac{\partial P_0^{[\mathrm{I}]}}{\partial T} - \frac{\partial}{\partial\eta}\left[V_1(\eta)P_0^{[\mathrm{I}]} - D_1\frac{\partial P_0^{[\mathrm{I}]}}{\partial\eta}\right] \quad (67)$$

Using the coefficients $V_0(\eta)$ and $D_0(\eta)$ from Eqs. (59) and (61) in Eq. (66), the leading-order quasi-steady solution is found to be a symmetric Gaussian peak.

$$P_0^{[\mathrm{I}],\infty}(\eta,T) = A(T)\left(\frac{2k\gamma}{\sqrt{\pi}}\right)\mathrm{e}^{-(2k\gamma\eta)^2} \quad (68)$$

where $A(T)$ represents the total probability contained within the leading-order peak, as before. The analog of Eq. (34) is

$$A'(T) = \left[V_0(\eta)P_1^{[\mathrm{I}]} - D_0\frac{\partial P_1^{[\mathrm{I}]}}{\partial\eta}\right]_{-\infty} \quad (69)$$

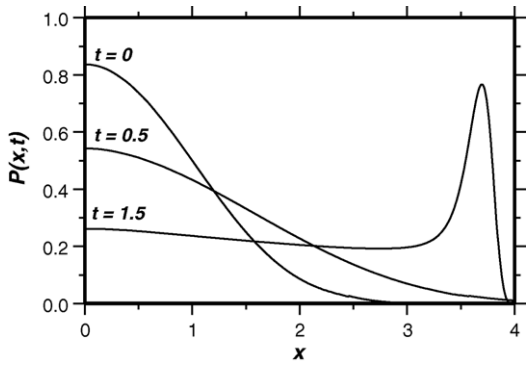

Fig. 5. Numerical PDF's for a FENE dumbbell with variable drag (Eq. (48)). Here, $\gamma = 1$, $\epsilon = 0.25$ and $k = \sqrt{2}/2$.

From this we find the asymptotic decay of the inner solution:

$$P_1^{[\mathrm{I}],\infty}(\eta, T) \sim -\left[\frac{A'(T)}{4k\gamma^2}\right]\frac{1}{\eta} \quad \text{as } \eta \to \infty \tag{70}$$

That $P_1^{[\mathrm{I}],\infty}$ should vanish in the outer limit could have been anticipated from the fact that there is no ord(1) contribution in the inner limit of the outer solution. The zeroth-order inner solution $P_0^{[\mathrm{I}],\infty}(\eta, T)$ suffices for calculating integral properties at leading order.

4.3. Summary of the inner solution

Thus far, we have uncovered a boundary-layer structure that is similar to that for dumbbell Model A, in that it is a peak of ord(ϵ) width. The main differences are:

- Its Gaussian shape (68), as opposed to the asymmetric exponential profile (32).
- Its location centered at $x = \lambda$ (Eq. (52)), slightly inboard from the limit of extension $x = \epsilon^{-1}$.
- A smaller disparity between the inner and outer timescales (cf. Eqs. (26) and (64)).

These features (confirmed by the numerical PDF's shown in Fig. 5) will not hinder applicability of the L closure.

4.4. A Peterlin-type closure

Compared with the exactly solvable case of Eq. (5), the FENE and configuration-dependent drag factors in Eq. (48) bring a significant complication. The ODE (14) is no longer closed

$$\frac{\mathrm{d}\langle x^2\rangle}{\mathrm{d}t} = 2\gamma\langle x^2\rangle - \left\langle \frac{x^2}{(1+kx)(1-\epsilon^2x^2)}\right\rangle + \frac{1}{\langle x^2\rangle}\left\langle\frac{x^2}{1+kx}\right\rangle \tag{71}$$

because the averages of the velocity and diffusivity can no longer be evaluated directly in terms of the second moment being solved for. Additional information is required, and this is often supplied in the form of the Peterlin approximation [1,7,15]—an assumed, approximate interchangeability of the order of taking the ensemble average (integral against the PDF) and nonlinear algebraic

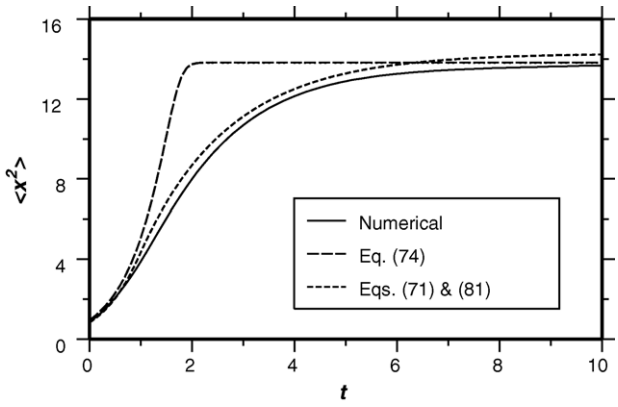

Fig. 6. Time evolution of the second moment for a FENE dumbbell with variable drag, corresponding to Fig. 5. Numerical results are compared with the Peterlin-type closure (74) and the L closure [8] (Eqs. (71) and (81)).

operations:

$$\langle 1\rangle \overset{\text{def}}{=} \left\langle \frac{x^2}{1+kx}\right\rangle \approx \frac{\langle x^2\rangle}{1+k\sqrt{\langle x^2\rangle}} \tag{72}$$

$$\langle 2\rangle \overset{\text{def}}{=} \left\langle \frac{x^2}{(1+kx)(1-\epsilon^2x^2)}\right\rangle \approx \frac{\langle x^2\rangle}{(1+k\sqrt{\langle x^2\rangle})(1-\epsilon^2\langle x^2\rangle)} \tag{73}$$

More expedient than mathematically justifiable, this approach has been widely used in polymer kinetic theory. In any case, the ODE for the second moment is now closed:

$$\frac{\mathrm{d}\langle x^2\rangle}{\mathrm{d}t} = 2\gamma\langle x^2\rangle - \frac{\langle x^2\rangle}{(1+k\sqrt{\langle x^2\rangle})(1-\epsilon^2\langle x^2\rangle)} + \frac{1}{1+k\sqrt{\langle x^2\rangle}} \tag{74}$$

Fig. 6 compares the time dependence of the second moment as calculated from this ODE with the numerical results. Although the FENE factor causes $\langle x^2\rangle$ to level off of its own accord (in contrast to the consistently averaged curve in Fig. 2), the intermediate rise is still much too rapid, and the curve again bends too abruptly toward the final steady asymptote. The obvious culprits are the closure assumptions (72) and (73). Their validity is not a matter of speculation or convenience: it depends on the actual PDF's, and can be checked directly against the numerical solution of the Smoluchowski equation (48). This comparison is made in Fig. 7 and Fig. 8. Each point on the numerical curves corresponds to a particular time in the family of PDF's (Fig. 5), at which the second moment was calculated and plotted as the abscissa. While the first Peterlin-type closure assumption (72) is surprisingly accurate, the second one (73) gives an entirely wrong shape at large extensions. Nevertheless, Eq. (73) is seen to be accurate at one special point: $\langle x^2\rangle$=λ^2, which is the final steady-state (at leading order) for the stretched FENE dumbbell. That is why steady-state properties can be accurately modeled with the Peterlin-type closure, even though the transient properties are poorly predicted. This fortunate intersection of the actual and Peterlin curves is not coincidental, as will be seen in the next section.

4.5. The L closure

As with the linear-locked dumbbell, a single Gaussian peak cannot sufficiently capture the transient structure of the actual PDF: a spreading central core that drains into an accumulating boundary layer near the limit of extension. Thus, we are led to consider a slightly modified version of Eq. (44), in which the location of the inner spike is suitably modified according to Eq. (52).

$$P_{\mathrm{L}}(x,t) = \begin{cases} \lambda^{-1} Q[H(x) - H(x-\lambda Q^{-1})], & Q \geq 1 \\ \lambda^{-1} Q[H(x) - H(x-\lambda)] + (1-Q)\delta(x-\lambda), & 0 \leq Q < 1 \end{cases} \tag{75}$$

This simple form allows the integrals on the left-hand sides of Eqs. (72) and (73) to be evaluated analytically, and gives a linear dependence upon Q when $Q < 1$.

$$\langle j \rangle_{\mathrm{L}} = \begin{cases} \alpha_j(\lambda Q^{-1}), & Q \geq 1 \\ \beta_j(\lambda) + [\alpha_j(\lambda) - \beta_j(\lambda)]Q, & 0 \leq Q < 1 \end{cases} \tag{76}$$

with

$$\alpha_1(x) = \frac{1}{xk^3}\left\{\ln(1+kx) - kx + \frac{k^2x^2}{2}\right\} \tag{77}$$

$$\beta_1(x) = \frac{x^2}{1+kx} \tag{78}$$

$$\alpha_2(x) = \frac{1}{x}\left\{\frac{\ln(1+kx)}{k(k^2-\epsilon^2)} - \frac{\ln(1+\epsilon x)}{2\epsilon^2(k-\epsilon)} - \frac{\ln(1-\epsilon x)}{2\epsilon^2(k+\epsilon)}\right\} \tag{79}$$

$$\beta_2(x) = \frac{x^2}{(1+kx)(1-\epsilon^2x^2)} \tag{80}$$

Upon relating Q to the second moment by the applicable analog of Eq. (45), we find the closure relation

$$\langle j \rangle_{\mathrm{L}} = \begin{cases} \alpha_j(\sqrt{3\langle x^2\rangle}), & 0 \leq \langle x^2\rangle \leq \frac{\lambda^2}{3} \\ \frac{3}{2}\left[1 - \frac{\langle x^2\rangle}{\lambda^2}\right]\alpha_j(\lambda) + \left[-\frac{1}{2} + \frac{3}{2}\frac{\langle x^2\rangle}{\lambda^2}\right]\beta_j(\lambda), & \frac{\lambda^2}{3} \leq \langle x^2\rangle \leq \lambda^2 \end{cases} \tag{81}$$

Note in particular the two endpoints of the linear segment of the curve:

$$\langle j \rangle_{\mathrm{L}} = \alpha_j(\lambda) \quad \text{when } \langle x^2\rangle = \frac{1}{3}\lambda^2,$$
$$\langle j \rangle_{\mathrm{L}} = \beta_j(\lambda) \quad \text{when } \langle x^2\rangle = \lambda^2 \tag{82}$$

These approximations are plotted in Figs. 7 and 8, and agree very closely with the numerical results, especially where the dumbbell is appreciably stretched out. Substituting the new closure relations (81) into the second-moment ODE (71), we obtain much more accurate results for the transient behavior of $\langle x^2\rangle$, as compared with the Peterlin-type closures (72) and (73) (see Fig. 6).

Eq. (81) happens to coincide *precisely* with the Peterlin-type closures (72) and (73) when $\langle x^2\rangle = \lambda^2$, because at this one point all of the probability has drained into the delta function spike in the simplified PDF (75) (cf. Eqs. (78), (80) and (82)). This explains the fortuitous success of the Peterlin-type closures (only) for the *steady-state* properties. It should be noted, however, that the Peterlin curve will not level off *exactly* at $\langle x^2\rangle = \lambda^2$, because the steady-state version of the ODE (74)

$$\gamma - \frac{1}{2}\left(\frac{1}{1+k\sqrt{\langle x^2\rangle}}\right)\left(\frac{1}{1-\epsilon^2\langle x^2\rangle}\right) + \frac{1}{2\langle x^2\rangle} \times \left(\frac{1}{1+k\sqrt{\langle x^2\rangle}}\right) = 0 \tag{83}$$

adds to the two convective terms from Eq. (51) a third, diffusive term of order ϵ^2. As the final steady state is slightly displaced from intersection between the Peterlin and L closure curves in Figs. 7 and 8, the two approximations will have diverged from each other. This is why the long-time asymptotes in Fig. 6 differ marginally.

For the boundary-layer accumulation we note the following analog of Eq. (46), which can be derived from the box-spike shape of the PDF: (75).

$$A = \begin{cases} 0, & 0 \leq \langle x^2\rangle \leq \frac{\lambda^2}{3} \\ -\frac{1}{2} + \frac{3}{2}\frac{\langle x^2\rangle}{\lambda^2}, & \frac{\lambda^2}{3} \leq \langle x^2\rangle \leq \lambda^2 \end{cases} \tag{84}$$

Finally, in view of Eqs. (52), (77)–(80), the linear portion of the closure relation (81) yields the following leading-order asymptotic forms as $\epsilon \to 0$:

$$\left\langle \frac{x^2}{1+kx} \right\rangle \sim \frac{1}{k\epsilon}\left[\frac{1}{4} + \frac{3}{4}\epsilon^2\langle x^2\rangle\right] \tag{85}$$

$$\left\langle \frac{x^2}{(1+kx)(1-\epsilon^2x^2)} \right\rangle \sim \frac{2\gamma}{\epsilon^2}\left[-\frac{1}{2} + \frac{3}{2}\epsilon^2\langle x^2\rangle\right] \tag{86}$$

for $1/3 \leq \epsilon^2\langle x^2\rangle \leq 1$.

5. Transient stresses

In order to compute the stress, the Smoluchowski equations (5) and (48) can be summarized in the encompassing form

$$\frac{\partial P}{\partial t} + \frac{\partial}{\partial x}\left\{P\left[\gamma x - \frac{1}{2}\frac{F_{\{P\}}(x)}{\zeta(x)}\right]\right\} = 0 \tag{87}$$

where the driving force $F_{\{P\}}(x)$ consists of an enthalpic contribution (spring) and an entropic contribution (diffusion):

$$F_{\{P\}}(x) = f(x) + \frac{\partial \ln P}{\partial x} \tag{88}$$

The spring laws and friction coefficients for the two dumbbell models are

$$f(x) = x, \qquad \zeta(x) = 1 \quad \text{(Model A)} \tag{89}$$

$$f(x) = x(1-\epsilon^2x^2)^{-1}, \quad \zeta(x) = 1 + kx \quad \text{(Model B)} \tag{90}$$

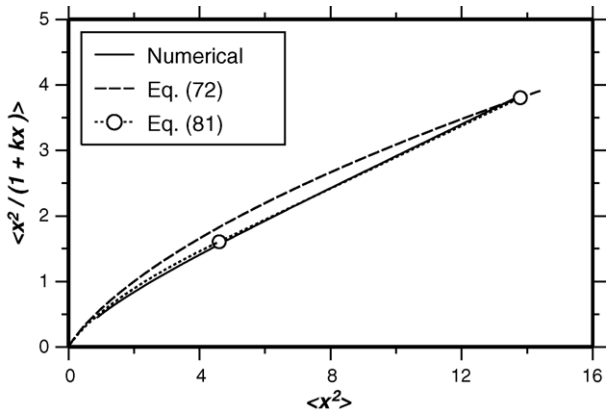

Fig. 7. Averages of the diffusion term in the second-moment ODE (71). Integrals of the numerical PDF's from Fig. 5 are compared with the Peterlin-type closure (72) and the L closure (81).

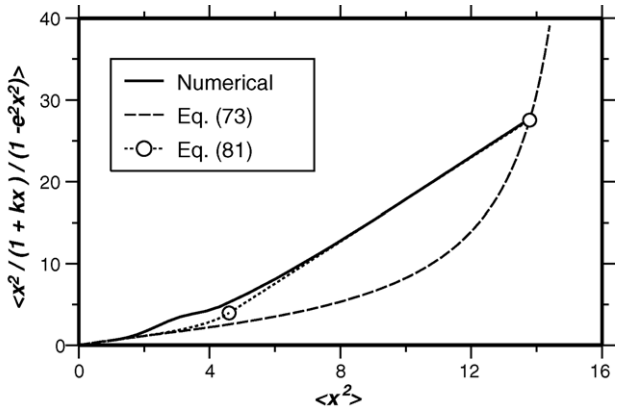

Fig. 8. Averages of the spring term in the second-moment ODE (71). Integrals of the numerical PDF's from Fig. 5 are compared with the Peterlin-type closure (73) and the L closure (81).

The contribution of one dumbbell to the stress in the polymer solution is given by a weighted average of the driving force,

$$\tau(t) = \int_0^{\epsilon^{-1}} xPF_{\{P\}}(x)\,\mathrm{d}x \tag{91}$$

The factor xP in this integral is proportional to the number density of dumbbells stretched to length x that cut across a given plane.

5.1. Linear-locked dumbbell with fixed friction

In the case of the linear-locked dumbbell there is a contribution to the stress from the hard stop of the spring at $x = \epsilon^{-1}$. This can be seen by adding to the driving force (88) a force term due to an infinitely high, soft potential barrier operative on a very short lengthscale that is negligible compared to the ord(ϵ) boundary-layer thickness described in Section 3.4.

$$\hat{F}_{\{P\}}(x) = x + \frac{\partial \ln P}{\partial x} + \frac{\mathrm{d}\Phi}{\mathrm{d}x} \tag{92}$$

For this vanishingly thin potential zone an inner/two-time analysis similar to that presented in Sections 3.5 and 4.2 shows that the near-wall PDF rapidly equilibrates to the Boltzmann distribution

$$\hat{P}(x,t) \sim P(\epsilon^{-1},t)\,\mathrm{e}^{-\Phi(x)} \tag{93}$$

Integrating xP against the new driving force gives

$$\epsilon^2\tau(t) = \epsilon^2(\langle x^2\rangle - 1) + 2\epsilon P(\epsilon^{-1},t) \sim \epsilon^2\langle x^2\rangle + (4\gamma - 2)A(t) \tag{94}$$

at leading order.

Running through the intermediate parameter Q defined by Eq. (42), the asymptotic stress–extension curve can be obtained by plotting the reduced stress,

$$\epsilon^2\tau \sim \left(\frac{2}{\pi Q^2}\right)\mathrm{erf}\left(\frac{Q\sqrt{\pi}}{2}\right) - \left(\frac{2}{\pi Q}\right)\exp\left(\frac{-\pi Q^2}{4}\right) + (4\gamma - 1)\,\mathrm{erfc}\left(\frac{Q\sqrt{\pi}}{2}\right) \tag{95}$$

against the reduced second moment from Eq. (43). The corresponding (piecewise-linear) formula for the L closure results from inserting Eq. (46) into (94):

$$\epsilon^2\tau = \begin{cases} \epsilon^2\langle x^2\rangle, & 0 \le \epsilon^2\langle x^2\rangle \le \frac{1}{3} \\ (1-2\gamma) + (6\gamma - 2)\epsilon^2\langle x^2\rangle, & \frac{1}{3} \le \epsilon^2\langle x^2\rangle \le 1 \end{cases} \tag{96}$$

These two curves are compared in Fig. 9, for $\gamma = 1$.

5.2. FENE dumbbell with variable friction

Since the probability density vanishes at the limit of extension (where the nonlinear Warner restoring force blows up), the one-dimensional version of the standard Kramers formula [1,7–9,16] applies for the stress.

$$\tau(t) = \int_0^{\epsilon^{-1}} P(x,t)xf(x)\,\mathrm{d}x - 1 \tag{97}$$

The boundary-layer contribution to the stress dominates for the FENE dumbbell with variable friction. Near $x = \lambda$ the spring-force factor is

$$xf(x) = \frac{x^2}{1 - \epsilon^2 x^2} = \frac{2k\gamma}{\epsilon^3} + \mathrm{O}(\epsilon^{-2}) \tag{98}$$

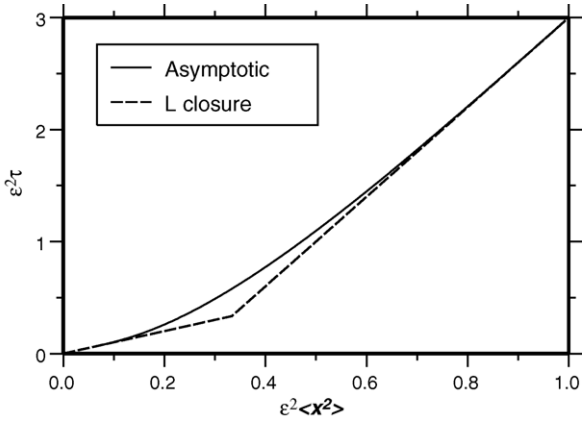

Fig. 9. Stress–extension curves for the linear-locked dumbbell with fixed drag in suddenly started uniaxial extension.

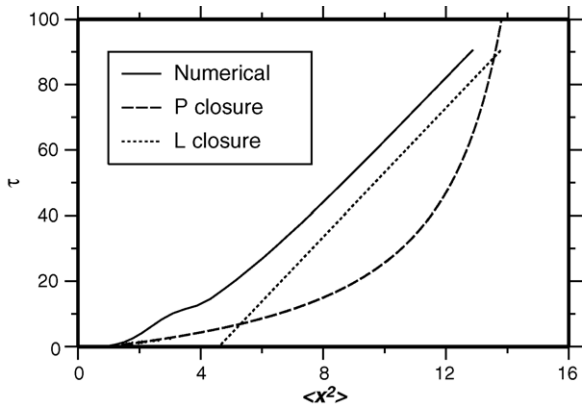

Fig. 10. Stress–extension curves for the FENE dumbbell with variable drag in suddenly started uniaxial extension. Here, $\gamma = 1$, $\epsilon = 0.25$ and $k = \sqrt{2}/2$.

The leading-order stress is then found to be

$$\epsilon^2 \tau(t) \sim \frac{2k\gamma}{\epsilon} A(t) \tag{99}$$

with A given in terms of $\langle x^2 \rangle$ by Eq. (84). Thus, the L closure yields the following stress–extension curve:

$$\epsilon^2 \tau \sim \begin{cases} 0, & 0 \le \langle x^2 \rangle \le \frac{\lambda^2}{3} \\ \frac{2k\gamma}{\epsilon}\left[-\frac{1}{2} + \frac{3}{2}\frac{\langle x^2 \rangle}{\lambda^2}\right], & \frac{\lambda^2}{3} \le \langle x^2 \rangle \le \lambda^2 \end{cases} \tag{100}$$

with λ being given by Eq. (52). Fig. 10 shows that this analytical formula compares much better with the corresponding curve from the numerical solution than does the Peterlin closure.

Note the ord(ϵ^{-1}) scaling in Eq. (100), whereby stresses can build up to much higher values than for the linear-locked dumbbell with fixed friction, when the extensibility parameter is large (cf. Eq. (96)).

6. Concluding remarks

This paper has applied the L closure of Lielens and coworkers [8,9,16], which was originally developed for FENE dumbbells with fixed friction, to two alternative dumbbell models of polymers in a dilute solution undergoing uniaxial extension: a linear-locked dumbbell with fixed friction (Model A) and a FENE dumbbell with variable friction (Model B). The two main features of the simplified PDF shape associated with the L closure have been examined with reference to the full PDF, as established with: (i) numerical solution via an atomistic SPH method [10,29] and (ii) asymptotic analysis for the limit of a large extensibility parameter at fixed elongation rate. Flatness of the spreading central core of probability density, when the dumbbell gets significantly extended, justifies the rectangular portion of the simplified PDF. An asymptotically narrow spike in probability density at or near the limit of extension motivates the terminal delta function. It is noted that the FENE dumbbell with fixed friction does *not* possess the required asymptotic structure [29], and is therefore less amenable to the L closure than the FENE with variable friction. Only with increased frictional grip of the fluid on the dumbbell as the latter becomes extended does advection dominate over diffusion to confine the accumulated probability near the end within a thin boundary layer. There is a separation of timescales, whereby the boundary layer equilibrates rapidly to the relatively slow outflux of probability toward the end. To address this behavior, singular perturbation analysis was combined with the method of multiple scales. The location of the boundary layer (terminal spike) remains fixed as the dumbbell gets stretched, which fixes one of the two state variables in the L closure, and thereby reduces it to first order.

For dumbbell Model A we have obtained a uniformly valid asymptotic approximation for the full PDF, which compares well with the numerical solution even for a relatively short dumbbell. The outer solution (spreading central core of probability) is exactly a Gaussian distribution, which is not constrained by the hard stop in the spring and (in the absence of the boundary layer) would allow a finite probability beyond the limit of extension. A Taylor expansion of this Gaussian profile leads precisely to the rectangular portion of the L closure PDF. The inner solution takes whatever probability *would have* accumulated beyond the limit of extension, and piles it up in an asymptotically narrow, exponential (Boltzmann) distribution against the stop in the spring. The finite probability density at the end contributes to the stress.

For dumbbell Model B we have pursued the asymptotics far enough to establish the leading-order behavior of the inner solution, which is an asymptotically narrow Gaussian peak centered inboard of the limit of extension, precisely where the spring's restoring force balances the stretching influence of the elongational flow, and the advective velocity vanishes. In contracting the Smoluchowski equation to its second-moment form, the conformational averages of two specific nonlinear expressions must be closed in terms of the second moment. For these quantities, the simplified, L closure shape of the PDF is analytically tractable, and yields closure functions that are actually linear in the regime of significant stretching. These closure laws (validated against numerical results based upon the full PDF) show why the applicable form of the Peterlin closure [13,15,7,8] should be accurate at the final steady state, while seriously missing the intervening transients. In the limit of a large extensibility parameter (in which the L closure is asymptotically justified), we obtain appealingly simple expressions for the coefficients in the closure functions.

Example calculations for a moderate (dimensionless) limit of extension ($L = 4$) show the L closure to yield reasonably accurate stress–extension curves for both dumbbell models, to which it had previously not been applied. Stresses for Model B can reach much higher levels than for Model A, as is explained by the asymptotic scaling.

Finally, as an effort toward completeness, we compare the L closure to two simpler modifications of the original Peterlin closure, which have thus far been applied to the FENE dumbbell with fixed friction (as opposed to the case of variable friction treated here) in an attempt to improve the predictions of transient stresses and hysteresis. The FENE-P* closure [22] regarded the extensibility parameter and relaxation time (equivalently, our L and γ) as adjustable fitting parameters in the FENE-P model—using new values L' and γ' to match the shear modulus and steady zero-shear-rate viscosity of the corresponding full FENE described by given L and γ. Thereby, L' was reduced to less than

66% of L. Improvements in the predictions of initial build-up of the elongational viscosity were offset by terminal asymptotes that were much too low. This trade-off highlights the limitation of lumping the outflowing probability together (effectively in a delta function spike), so that it must arrive all at once near the limit of extension—however that parameter is chosen. The second-order FENE-P^2 closure [8] distributed the total probability between two delta function spikes: (i) the movable peak from the FENE-P and (ii) an additional spike confined to zero extension. This simple representation of the PDF was, in principle, able to represent the drainage of probability from a grossly stylized central core into an accumulating peak at larger extensions. Evolution equations for the second and fourth moments were closed in terms of the two independent shape parameters (location α of, and amount β of probability in, the movable spike). In implementing this idea, however, an initially unexpected degeneracy surfaced, whereby the two moments (state variables) ended up being connected by an additional constraint. Thus, the FENE-P^2 approach reduced to a first-order FENE-P closure with a reduced extensibility parameter, which made it essentially equivalent to the FENE-P*.

Throughout the start-up of elongational flow, our asymptotic analysis shows the location of the boundary layer (stylized in the L closure as a delta function spike) to remain fixed while the time-evolving PDF drains probability from the central core (stylized as a rectangle) into the boundary layer. Thus, the L closure also reduces to first order. But the resulting second moments and stresses are substantially more accurate than for the FENE-P^2 [8].

Acknowledgements

LCN would like to thank Professor E.J. Hinch, DAMTP, University of Cambridge, UK, for a series of very helpful conversations during the early stages of this work. LEW is grateful for the support of the 3M Company.

References

[1] R.B. Bird, C.F. Curtiss, R.C. Armstrong, O. Hassager, Dynamics of Polymeric Liquids: Vol. 2, Kinetic Theory, second ed., Wiley/Interscience, New York, 1987.
[2] P.G. DeGennes, Coil-stretch transition of dilute flexible polymer under ultrahigh velocity gradients, J. Chem. Phys. 60 (1974) 5030–5042.
[3] C.W. Gardiner, Handbook of Stochastic Methods, third ed., Springer, Berlin, 2004.
[4] E.J. Hinch, Mechanical models of dilute polymer solutions in strong flows, Phys. Fluids 20 (1977) S22–S30.
[5] P. Ilg, I.V. Karlin, H.C. Öttinger, Canonical distribution functions in polymer dynamics. I. Dilute solutions of flexible polymers, Physica A 315 (2002) 367–385.
[6] P. Ilg, I.V. Karlin, M. Kröger, H.C. Öttinger, Canonical distribution functions in polymer dynamics. II. Liquid–crystalline polymers, Physica A 319 (2003) 134–150.
[7] R. Keunings, On the Peterlin approximation for finitely extensible dumbbells, J. Non-Newtonian Fluid Mech. 68 (1997) 85–100.
[8] G. Lielens, P. Halin, I. Jaumain, R. Keunings, V. Legat, New closure approximations for the kinetic theory of finitely extensible dumbbells, J. Non-Newtonian Fluid Mech. 76 (1998) 249–279.
[9] G. Lielens, R. Keunings, V. Legat, The FENE-L and FENE-LS closure approximations to the kinetic theory of finitely extensible dumbbells, J. Non-Newtonian Fluid Mech. 87 (1999) 179–196.
[10] L.C. Nitsche, W. Zhang, Atomistic SPH and a link between diffusion and interfacial tension, AIChE J. 48 (2002) 201–211.
[11] H.C. Öttinger, A model of dilute polymer solutions with hydrodynamic interaction and finite extensibility. I. Basic equations and series expansions, J. Non-Newtonian Fluid Mech. 26 (1987) 207–246.
[12] H.C. Öttinger, Stochastic Processes in Polymeric Fluids, first ed., Springer, Berlin, 1996.
[13] A. Peterlin, Hydrodynamics of macromolecules in a velocity field with longitudinal gradient, J. Polym. Sci. Polym. Lett. 4B (1966) 287–291.
[14] J.M. Rallison, E.J. Hinch, Do we understand the physics in the constitutive equation? J. Non-Newtonian Fluid Mech. 29 (1988) 37–55.
[15] P. Singh, L.G. Leal, Computational studies of the FENE dumbbell model with conformation-dependent friction in a co-rotating two-roll mill, J. Non-Newtonian Fluid Mech. 67 (1996) 137–178.
[16] R. Sizaire, G. Lielens, I. Jaumain, R. Keunings, V. Legat, On the hysteretic behaviour of dilute polymer solutions in relaxation following extensional flow, J. Non-Newtonian Fluid Mech. 82 (1999) 233–253.
[17] A.J. Szeri, A deformation tensor model for nonlinear rheology of FENE polymer solutions, J. Non-Newtonian Fluid Mech. 92 (2000) 1–25.
[18] R.I. Tanner, Stresses in dilute solutions of bead-nonlinear-spring macromolecules. II. Unsteady flows and approximate constitutive relations, Trans. Soc. Rheol. 19 (1975) 37–65.
[19] R.I. Tanner, Stresses in dilute solutions of bead-nonlinear-spring macromolecules. III. Friction coefficient varying with dumbbell extension, Trans. Soc. Rheol. 19 (1975) 557–582.
[20] R.I. Tanner, Engineering Rheology, second ed., Oxford University Press, New York, 2000.
[21] R.I. Tanner, W. Stehrenberger, Stresses in dilute solutions of bead-nonlinear-spring macromolecules. I. Steady potential and plane flows, J. Chem. Phys. 55 (1971) 1958–1964;
R.I. Tanner, W. Stehrenberger, Stresses in dilute solutions of bead-nonlinear-spring macromolecules. I. Steady potential and plane flows, J. Chem. Phys. 61 (1974) 2486 (Erratum).
[22] A.P.G. van Heel, M.A. Hulsen, B.H.A.A. van den Brule, On the selection of parameters in the FENE-P model, J. Non-Newtonian Fluid Mech. 75 (1998) 253–271.
[23] V. Verleye, F. Dupret, Prediction of fibre orientation in complex injection moulded parts, in: C.E. Altan, D.A. Siginer, W.E. Van Arsdale, A.N. Alexandrou (Eds.), Developments in Non-Newtonian Flows, AMD, vol. 175, ASME, New York, 1993, pp. 139–163.
[24] H.R. Warner, Kinetic theory and rheology of dilute suspensions of finitely extendible dumbbells, Ind. Eng. Chem. Fundam. 11 (1972) 379–387.
[25] L.E. Wedgewood, A Gaussian closure of the second-moment equation for a Hookean dumbbell with hydrodynamic interaction, J. Non-Newtonian Fluid Mech. 31 (1989) 127–142.
[26] L.E. Wedgewood, R.B. Bird, From molecular models to the solution of flow problems, Ind. Eng. Chem. Res. 27 (1988) 1313–1320.
[27] L.E. Wedgewood, H.C. Öttinger, A model of dilute polymer solutions with hydrodynamic interaction and finite extensibility. II. Shear flows, J. Non-Newtonian Fluid Mech. 27 (1988) 245–264.
[28] J.M. Wiest, L.E. Wedgewood, R.B. Bird, On coil-stretch transitions in dilute polymer solutions, J. Chem. Phys. 90 (1989) 587–594.
[29] W. Zhang, Particle methods and perturbation theory in transport phenomena: polymer rheology and membrane separations, Ph.D. Thesis, University of Illinois at Chicago, 2004.
[30] Q. Zhou, R. Akhavan, Cost-effective multi-mode FENE bead-spring models for dilute polymer solutions, J. Non-Newtonian Fluid Mech. 116 (2004) 269–300.
[31] B.H. Zimm, Dynamics of polymer molecules in dilute solution: viscoelasticity, flow birefringence and dielectric loss, J. Chem. Phys. 24 (1956) 269–278.
[32] W. Zylka, H.C. Öttinger, A comparison between simulations and various approximations for Hookean dumbbells with hydrodynamic interaction, J. Chem. Phys. 90 (1989) 474–480.